AIAA JOURNAL
Vol. 37, No. 5, May 1999

Coupled Thermal Model for Nonlinear Panel Flutter

D. J. Gee* and S. R. Sipcic†
Boston University, Boston, Massachusetts 02215

A nonlinear formulation is developed that accounts for high-Mach-number, viscous flow over the external surface of an isotropic elastic panel. The formulation is unique in that the panel compressive stress is calculated as a result of fluid/structure thermal coupling. Two distinct heat transfer mechanisms are investigated. One is due to fluid viscosity, and the second is due to local flow over the panel. Here, in contrast with classical panel flutter studies, the in-plane load and dynamic pressure parameters are not wholly independent parameters. The equation of motion is based on von Kármán large deflection plate theory and includes a geometric nonlinearity. Using Galerkin's method, the resulting system of equations is solved by direct numerical integration. However, the parameter space representing the in-plane load is extensive, and therefore, numerical integration alone is not a feasible analysis method. As a supplement, the system of equations is analysed with a pseudoarclength continuation method. In this way, a new periodic regime is uncovered. However, the attractor becomes unstable as a result of additional heating. The results indicate that aerodynamic heating is the dominant heat transfer mechanism. For the conditions studied, the dynamic system is dominated by a stable fixed-point attractor. The aerothermoelastic panel flutter model formulated here is qualitatively similar to the classical model when the in-plane load is due to aerodynamic heating effects only.

Nomenclature

A = area element
a = reference length
c_p, c_v = specific heat at constant pressure, volume
c_∞ = speed of sound
D = cylindrical stiffness, $Eh^3/12(1-\nu^2)$
E = Young's modulus
h = panel thickness; also heat transfer coefficient
k_s = support stiffness
M = Mach number
Pr = Prandtl number, $\mu c_p/\kappa$
p = pressure
q = dynamic pressure, $\rho U^2/2$
R = ratio of panel-to-support axial rigidity, $(EA)_p/(EA)_s$
R_f = steady temperature recovery factor
R_u = unsteady temperature recovery factor
T = temperature
T_f = temperature due to aerodynamic heating
U_∞ = reference velocity
u, v = streamwise and normal velocity, respectively; also longitudinal displacement
w = transverse displacement
x, y = streamwise and normal coordinates, respectively
α = coefficient of thermal expansion
α_D = thermal diffusivity
β_k = support structure stiffness parameter, $1 + k_s a/(EA)_s$
γ = c_p/c_v
ϵ_x = strain component
κ = fluid thermal conductivity
λ = dynamic pressure parameter, $2q_\infty a^3/(M_\infty D)$
μ = $\rho_\infty a/(\rho_p h)$; also dynamic viscosity
ν = Poisson ratio
ρ = density
σ_x = stress component
$(\,)$ = $\mathrm{d}(\,)/\mathrm{d}t$
$(\,)_{,x}$ = $\partial(\,)/\partial x$

Subscripts

p = panel characteristic
s = support structure characteristic
u = condition at external surface

Received Dec. 22, 1997; revision received Nov. 3, 1998; accepted for publication Jan. 12, 1999.

*Graduate Researcher, Department of Aerospace and Mechanical Engineering; currently Postdoctoral Fellow, Institute for Advanced Technology, University of Texas at Austin, Austin, TX 78759. Member AIAA.

†Assistant Professor, Department of Aerospace and Mechanical Engineering; currently Research Scientist, RWD Technologies, Inc., Columbia, MD 21044.

Introduction

AEROTHERMOELASTIC considerations are important in the design of space re-entry vehicles and high-speed aircraft. As the name suggests, aerothermoelasticity concerns elastic structures under the combined effects of aerodynamic, thermodynamic, inertial, and elastic forces. The mathematical modeling from first principles describing these interactions is a formidable task. Consequently, aerothermoelastic studies have been based on a number of simplifying assumptions.

Much of the early work on panel flutter was restricted to supersonic speeds. A thorough discussion of the fundamental aspects was given by Dugundji.[1] It was recognized that geometrical nonlinearities due to moderate plate deflections can play an important role in panel flutter. This led to a number of studies that emphasized the geometrically nonlinear aspects using a finite deflection plate theory combined with first-order piston theory[2] for generating the unsteady aerodynamic loads.[3–6] These studies showed that when geometrical nonlinearities are included, the linear stability boundary can be exceeded, thereby inducing stable limit cycle oscillations with finite amplitudes. Dowell[3,4] has shown that nonlinear panel flutter is capable of producing irregular behavior. More recently, the problem was examined in the context of chaos theory.[7] Related results were obtained in the presence of inertial forces due to maneuvering by Sipcic and Morino[8] and by Sipcic.[9] Hedgepeth[10] has shown that piston theory aerodynamics is adequate for obtaining unsteady aerodynamic loads when compared against higher-order aerodynamic methods such as aerodynamic surface theory. The influence of various orders of piston theory on the stability boundary and limit cycle amplitudes was studied by Bein et al.[11] It was found that for high Mach numbers, a numerical solution of the unsteady Euler equations gives virtually identical responses as those obtained with the simpler piston theory.

Fung[12] has considered the stability of an aerodynamically heated, isotropic, curved panel subject to high supersonic flow over one side. In this case, a stable static equilibrium is guaranteed for temperatures below the critical value. However, a nontrivial limit cycle is encountered for a panel temperature rise greater than the critical value. The effect of a parabolic temperature distribution was considered by Schaeffer and Heard.[13] It was shown that a nonlinear

temperature distribution may be as important in affecting panel flutter as a uniform compressive stress. Bein et al.[11] also found that aerodynamic heating has a strong influence both on the critical dynamic pressure, i.e., that for onset of linear instability, and on the amplitude of the limit cycle. In all of these studies, however, the temperature distribution was prescribed.

Several experimental studies have shown that compressive stress induced by aerodynamic heating could initiate flutter of a flat panel that would otherwise be stable.[14,15] Furthermore, the results showed that additional heating could stop the flutter. Guy and Bohon[15] conducted a series of experiments on two- and four-bay panels of aluminum alloy and of stainless steel. It was shown that as the thermal stress increased, increasing thickness was required to prevent flutter.

Aerothermoelastic Panel Flutter

The effect of panel heating is twofold. First, there is reduction in stiffness due to softening of the panel material; second, thermal stress is generated due to mismatch in thermal expansion coefficients of the panel and support structure. These effects, in turn, affect the static and dynamic behavior of the panel. Only the latter effect is studied here.

Consider a panel exposed to an external hypersonic flow of velocity U_∞ over one side as shown in Fig. 1. The cavity beneath the panel is internal to the flow. The governing differential equation for the panel transverse displacement should account for thermal stress created by the fluid/structure interaction. Unsteady aerodynamic pressure results from surface deformation. Elastic forces are included via the material strain-displacement model, and inertial forces are zero when the deflection is stationary. By combining a finite deflection plate theory with piston theory, the aeroelastic problem is formulated as one nonlinear integro partial differential equation (PDE) for the panel transverse displacement. However, the classical panel flutter model neglects aerodynamic heating and treats the two main parameters (in-plane load and a dynamic pressure parameter) as independent. In reality, these are coupled by thermal effects.

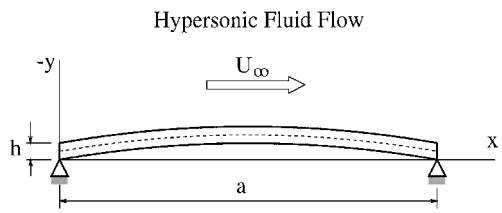

Fig. 1 Schematic of two-dimensional panel in hypersonic flow.

Two heat transfer mechanisms between the fluid and structure are considered. The first is due to viscous flow over the panel and is referred to as aerodynamic heating. It is assumed that the panel is exposed to airflow at constant speed for a sufficient time such that a steady-state temperature is established. Then, Crocco's solution of the boundary-layer equations determines the temperature increase due to viscous effects.[16] The second mechanism is inviscid in nature. It is assumed that the unsteady temperature and pressure above the panel are related via an isentropic flow relation. Next, an initial/boundary value problem (IBVP) is solved for the panel temperature distribution. The Duhamel superposition integral is a closed-form solution to this IBVP.[17] In this way, the temperature distribution is fully determined as a function of panel transverse motion. Note that panel in-plane heat conduction is not accounted for in the model. Next, thermal stress is computed as a function of the support structure stiffness. Finally, using von Kármán plate theory the equation of motion is formulated that takes into account the thermal modeling already described. The complete model is shown in Fig. 2.

Viscous Flow Model

For steady two-dimensional boundary-layer flow, the conservation equations may be given as

$$(\rho u)_{,x} + (\rho v)_{,x} = 0 \tag{1}$$

$$\rho(uu_{,x} + vu_{,y}) = -p_{,x} + (\mu u_{,y})_{,y} \tag{2}$$

$$\rho c_p(uT_{,x} + vT_{,y}) = up_{,x} + (\kappa T_{,y})_{,y} + \mu u_{,y}^2 \tag{3}$$

$$p = \rho RT \tag{4}$$

where Eq. (4) is an ideal gas relation. The pressure gradient is determined by the frictionless external flow. For flat plate, $p_{,x} = -\rho U_\infty (U_\infty)_{,x} = 0$. The applied boundary conditions may be given as

$$u = 0, \qquad T_{,y} = 0 \qquad \text{at} \qquad y = -h/2 \tag{5}$$

$$u \to U_\infty, \qquad T \to T_\infty \qquad \text{as} \qquad y \to -\infty \tag{6}$$

where $y = 0$ is the panel midplane and the positive y coordinate points downward. Then, given the fluid properties [$\mu = \mu(T)$, $\kappa = \kappa(T)$] one can solve Eqs. (1–4) for the four unknowns subject to Eqs. (5) and (6). Crocco has shown that, irrespective of the form of the viscosity function, the temperature as a solution of Eqs. (1–4)

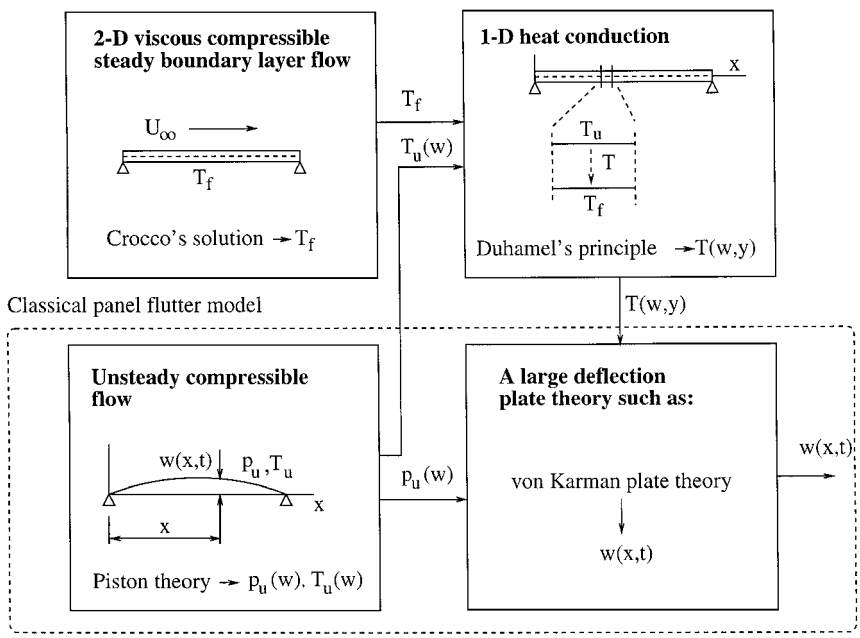

Fig. 2 Aerothermoelastic panel flutter.

depends solely on the velocity component parallel to the wall; i.e., $T = T(u)$. Hence, for the panel temperature one can show that

$$T_f - T_\infty = \Delta T_f = R_f[(\gamma - 1)/2]M_\infty^2 T_\infty \tag{7}$$

which follows with $M_\infty = U_\infty/c_\infty$ and $c_\infty^2 = (\gamma - 1)c_p T_\infty$. The recovery factor R_f ($=\sqrt{Pr}$) accounts for cases where Pr differs from unity.

Inviscid Flow Model

Piston theory is valid for $M_\infty \gg 1$. The aerodynamic loads due to panel transverse motion vary rapidly and result in nearly adiabatic conditions at the edge of the boundary layer. The pressure and temperature on the surface of a piston moving with velocity V may be given as

$$\frac{p_u}{p_\infty} = \left(1 + \frac{\gamma - 1}{2}\frac{V}{c_\infty}\right)^{\frac{2\gamma}{\gamma - 1}} \tag{8}$$

$$\frac{T_u}{T_\infty} = \left(1 + \frac{\gamma - 1}{2}\frac{V}{c_\infty}\right)^{2} \tag{9}$$

where Eq. (9) is obtained from Eq. (8) under the assumption that the pressure and temperature are related through an isentropic flow relation. The local transverse velocity may be expressed in terms of the panel transverse displacement $w(x, t)$ as

$$V = w_{,t} + U_\infty w_{,x} \tag{10}$$

Substituting Eq. (10) into Eqs. (8) and (9), the corresponding linear relations are

$$p_u - p_\infty = (2q_\infty/M_\infty)D_t w \tag{11}$$

$$T_u - T_\infty = (\gamma - 1)M_\infty T_\infty D_t w \tag{12}$$

where $D_t w \equiv V/U_\infty = w_{,x} + w_{,t}/U_\infty$. Equation (12) needs to be modified to account for the fluid layer adjacent to the surface being heated by viscous action. Therefore, it is assumed that

$$T_u = T_f + (\gamma - 1)M_\infty T_\infty D_t w \tag{13}$$

Thus, if the local velocity is zero, i.e., $D_t w = 0$, then $p_u = p_\infty$ and $T_u = T_f$.

For the temperature, an unsteady temperature recovery factor $R_u \in [0, 1]$ is introduced such that $R_u = 0$ corresponds to zero net heat transfer to the panel, whereas $R_u = 1$ implies perfect thermal communication between the fluid and panel. Consequently, the temperature change may be expressed as

$$T_u - T_f = \Delta T_u = R_u(\gamma - 1)M_\infty T_\infty D_t w \tag{14}$$

Note that ΔT_u can be positive or negative, whereas the temperature change due to aerodynamic heating is always positive. The surface pressure and temperature defined by Eqs. (11) and (14), respectively, are functions of the panel transverse motion through $w(x, t)$ only.

Heat Conduction Model

The temperature distribution through the panel is time dependent due to transverse motion. Heat conduction is governed by the one-dimensional heat conduction equation, which is given as

$$T_{,t} = \alpha_D T_{,yy} \tag{15}$$

Initially, the plate is assumed to be at constant temperature. For $t > 0$, the internal surface is maintained at temperature T_f, whereas the external surface varies in accordance with Eq. (14). These initial and boundary conditions may be stated as

$$T(x, y, 0) = T_f \tag{16}$$

$$T(x, h/2, t) = T_f \tag{17}$$

$$T(x, -h/2, t) = T_f + R_u(\gamma - 1)M_\infty T_\infty D_t w \tag{18}$$

The IBVP defined by Eqs. (15–18) contains a time-dependent boundary condition. The solution to this problem has been obtained previously by Duhamel and is given as

$$T(x, y, t) = T_f + \left[-(y/h) + \tfrac{1}{2}\right]\Delta T_u + T_t \tag{19}$$

where

$$T_t(x, y, t) = \frac{2}{\pi}\sum_{n=1}^{\infty}\frac{(-1)^n}{n}F\sin\left[n\pi\left(-\frac{y}{h} + \frac{1}{2}\right)\right]e^{-n^2 t/\zeta} \tag{20}$$

with

$$F = F\left(x, \frac{-h}{2}, t\right) = \Delta T_u^0 + \int_0^t (\Delta T_u)_{,\tau}\, e^{n^2\tau/\zeta}\, \mathrm{d}\tau \tag{21}$$

Here ζ ($= h^2/\alpha_D$) has units of time, and ΔT_u^0 is shorthand notation for $\Delta T_u(x, -h/2, 0)$. It is a straightforward procedure to show that the temperature given by Eq. (19) satisfies Eqs. (16–18).

A simplification to the preceding analysis is obtained by recalling some ideas on the convection and conduction of heat. Briefly, when the Biot number Bi [$= h(V/A)/k$] < 0.1, it is acceptable to analyze the temperature on a lumped-capacity type of thermal analysis.[18] That is, the panel material offers such small resistance to heat flow, with respect to the convection environment, that we may consider the temperature to be uniform throughout the panel thickness. Said in another way, the temperature gradient within the panel is negligible with respect to that at the surface. It can be shown that for the problem considered here, $Bi < 0.1$ (Ref. 19). Hence the panel temperature for a lumped-capacity thermal analysis may be expressed as

$$T(x, t) = T_f + \Delta T_u \tag{22}$$

Structural Dynamics

The equation of motion for zero aerodynamic damping results from equilibrium considerations and is given by[5]

$$M_{,xx} + (N + N^E)w_{,xx} + (p_l - p_u) - \rho_p h w_{,tt} = 0 \tag{23}$$

where N^E is an externally applied in-plane load. To generate the relation for $w(x, t)$, von Kármán large deflection plate theory for cylindrical bending is used. By virtue of the Kirchoff–Love hypothesis, the strain–displacement relation and the thermal Hooke's law relation may be expressed as

$$\epsilon_x = u_{,x} + \tfrac{1}{2}w_{,x}^2 - y w_{,xx} \tag{24}$$

$$\sigma_x = [E/(1 - \nu^2)][\epsilon_x - \alpha(1 + \nu)\Delta T], \qquad \Delta T = T - T_{\text{ref}} \tag{25}$$

where T_{ref} is a reference temperature. With these preparations, the axial force and bending moment are

$$\tilde{N} = -(Eh)_p \Delta\bar{T}_f\left[\alpha_p - \left(\frac{\alpha_s + R\alpha_p}{\beta_k + R}\right)\right] - N^E + \frac{Eh}{a(1 - \nu^2)}\int_0^a \left[\frac{1}{2}w_{,x}^2 - \alpha_p(1 + \nu)\bar{R}_u D_t w\right]\mathrm{d}x \tag{26}$$

$$M = -D w_{,xx} \tag{27}$$

where $\Delta\bar{T}_f = T_f - T_{\text{ref}}$ and $\bar{R}_u = R_u(\gamma - 1)M_\infty T_\infty$. Equation (26) accounts for partially restrained thermal expansion with respect to aerodynamic heating. The integral expression represents the familiar term due to curvature shortening and an unsteady thermal thrust term.[19] To complete the formulation, the pressure difference across the panel is expressed as

$$p_l - p_u = -(p_u - p_\infty) + \Delta p_{st} \tag{28}$$

where p_l denotes the internal cavity pressure. The first term is the aerodynamic pressure defined by Eq. (11), and the second term corresponds to the static pressure differential across the panel, i.e., $\Delta p_{st} = p_l - p_\infty$.

Substituting Eqs. (26–28), or appropriate derivatives, into the equilibrium expression, the nondimensional PDE for the panel transverse displacement may be given as

$$\frac{\partial^4 \tilde{w}}{\partial \tilde{x}^4} + R_x^E \frac{\partial^2 \tilde{w}}{\partial \tilde{x}^2} - 6\frac{\partial^2 \tilde{w}}{\partial \tilde{x}^2}\int_0^1 \left(\frac{\partial \tilde{w}}{\partial \tilde{x}}\right)^2 \mathrm{d}\tilde{x} + \frac{\partial^2 \tilde{w}}{\partial \tilde{t}^2} + \lambda \tilde{D}_t w + \Delta \tilde{T}_f \Theta \frac{\partial^2 \tilde{w}}{\partial \tilde{x}^2} + \frac{h}{a}\frac{\tilde{R}_u}{(1-\nu)}\frac{\partial^2 \tilde{w}}{\partial \tilde{x}^2}\int_0^1 \tilde{D}_t w \,\mathrm{d}\tilde{x} = \Delta \tilde{p}_{st} \tag{29}$$

The nondimensional variables are summarized in Appendix A. Boundary conditions are those for a simply supported panel, and the panel is considered to be initially displaced. Hence,

$$w(0,t) = w(a,t) = 0, \qquad w_{,xx}(0,t) = w_{,xx}(a,t) = 0 \tag{30}$$

$$w(x,0) = f(x), \qquad \dot{w}(x,0) = 0 \tag{31}$$

Note that, by setting both the steady and unsteady thermal terms to zero, i.e., $\Delta \tilde{T}_f = \tilde{R}_u = 0$, Eq. (29) is similar to the classical aeroelastic panel flutter equation.[3] Similarly, for $\tilde{R}_u = R_x^E = 0$, the resulting PDE is similar to the classical panel flutter equation with the significant difference that the in-plane load is now based on the flight conditions rather than on an externally applied in-plane load.

Galerkin's Method

Following Galerkin's method, $w(x,t)$ is first expressed as a modal expansion:

$$w(x,t) \simeq W_N(x,t) = \sum_{r=1}^{N} w_r(t)\sin(\pi r x) \tag{32}$$

This approximation is not exact. That is, the differential equation is not satisfied everywhere in the domain Ω, although, by construction, it is satisfied on the closure Γ of the domain. Furthermore, only a finite number of terms are retained in Eq. (32). Hence, $W_N(x,t)$ belongs to the linear subspace $\mathcal{C}_N^2$ contained within the space of admissible functions $\mathcal{C}^2$. Substituting Eq. (32) and appropriate derivatives into Eq. (29) produces the following representation in terms of the modal coordinates:

$$(\pi s)^4 w_s(t) - R_x^E(\pi s)^2 w_s(t) + 3\sum_k (\pi k)^2 w_k^2(t)(\pi s)^2 w_s(t) + \ddot{w}_s(t) + 2\lambda \sum_{k,k\neq s} \frac{sk}{s^2-k^2}[1-(-1)^{s+k}]w_k(t) + \left(\frac{\lambda\mu}{M_\infty}\right)^{\frac{1}{2}} \dot{w}_s(t) - \Delta T_f \Theta(\pi s)^2 w_s(t) - \frac{h}{a}\frac{\bar{R}_u}{(1-\nu)}\left(\frac{\mu}{\lambda M_\infty}\right)^{\frac{1}{2}} \sum_k \frac{[1-(-1)^k]}{(\pi k)}\dot{w}_k(t)(\pi s)^2 w_s(t) = 2\Delta p_{st}\frac{[1-(-1)^s]}{\pi s}, \qquad s = 1,2,\ldots \tag{33}$$

Note the tilde notation has been dropped for clarity. In Eq. (33), the cubic nonlinearity results from coupling between in-plane stretching and out-of-plane bending, whereas the quadratic nonlinearity results from the unsteady heating effect.

Results

In the numerical results, the recovery factors are varied independently. In this way, the exact panel temperature should lie in between the bounds established by the extremum for the recovery factors. By addressing the physical problem in this manner, the matter of the characteristic thermal time h^2/α_D is temporarily set aside. That is, when the ratio of the characteristic thermal time to the period of vibration is large, the unsteady heating effect may be negligible. Bifurcation diagrams, long-time histories, power spectra, and phase-plane plots are the tools used in studying the system. The phase plane represents the panel transverse displacement vs velocity, evaluated at $x/a = 0.75$. In previous analyses, this point was shown to correspond to the maximal deflection for the fluttering panel. The ordinate for the power spectral density P_w is plotted with a linear scale, whereas the abscissa gives a frequency index X such that

$$\tilde{f} = X/2m\,\Delta t \tag{34}$$

where $\tilde{f}$ is the nondimensional frequency. In this relation, m is an integer that controls the spectral resolution, and Δt is the sampling interval.

Whereas some variables are determined by the choice of material, others are influenced by the construction method of the panel and support structure. These include the axial rigidities of the panel and support structure and the support stiffness. The values taken here and material properties for Rene-41 are summarized in Appendix B (Table B1). Also for the case considered here ($R_x^E = 0$, $h/a = 0.004$, $M_\infty = 4$, $h_o = 15$ km, $\lambda = 52.6$, $\Delta p_{st} = 0$), $\Theta = 1 - (\alpha_s + R\alpha_p)/(\alpha_p(\beta_k + R)) = 0.463$. Note that Θ varies with the panel thickness through the parameter β_k. Six modes are retained in the basic model. Earlier studies have shown that two-mode models will give an incorrect flutter boundary, whereas four-mode results are essentially correct.

In the aerothermoelastic model developed here, the parameter $R_f \in [0, 1]$ determines, in large part, the magnitude of the thermal compressive stress. With respect to the external in-plane load of classical panel flutter studies, the axial thrust term here can be several orders of magnitude larger than previously considered. One consequence is that direct numerical integration over the entire relevant parameter space is not feasible. Essentially, the step-size requirement limits the usefulness of procedures such as fixed step-size Runge–Kutta methods. Hence a supplemental procedure must be found for aerothermoelastic studies.

Continuation Method

As indicated in the preceding section, the nondimensional in-plane load will vary over several orders of magnitude for $R_f \in [0, 1]$. This large variation in the physics of the problem exposes some numerical difficulties for a fixed-step-size Runge–Kutta method. One problem is that, in order to converge to the solution for even moderate values of the in-plane compressive stress, an extremely small integration time step must be used. This results in an error due to the method that is less than machine precision. For certain nonlinear ordinary differential equations (ODEs), an alternate method is pseudoarclength continuation (AUTO). Continuation methods, which can be thought of as predictor–corrector methods, show how solutions vary with a parameter. Briefly, a continuation method proceeds from a system of first-order differential equations containing at least one free parameter. Starting from a known solution, incrementing the free parameter introduces a perturbation to the vector field. In this way, the adjacent solution on the branch is sought. The step size is the pseudoarclength (in which the distance from the known solution to the next solution on the branch can include all state variables and free parameters). The predictor step is a low-order approximation to the branch. Next, each predictor step is corrected by iterating toward the branch with a Newton/Chord method. Local existence of the solution branch can be inferred with the Implicit Function Theorem. In this way, equilibrium solution branches are determined as the zeros of the vector field. Under certain conditions, the stability of the critical point $\bar{x}$ may be determined from the linear approximation or the linear variational equation about $\bar{x}$. That is, when $\bar{x}$ is a hyperbolic critical point, the linear variational equation is sufficient to determine stability. [For the differential equation $\dot{x} = f(\lambda, x)$, where λ is a parameter and $f(\lambda_o, \bar{x}) = 0$; $\bar{x}$ is called a hyperbolic critical point if $f'(\lambda_o, \bar{x}) \neq 0$. If $f'(\lambda_o, \bar{x}) = 0$, then $\bar{x}$ is called a nonhyperbolic or degenerate critical point; also, $\bar{x}$ is asymptotically stable if $f'(\lambda_o, \bar{x}) < 0$ and is unstable if $f'(\lambda_o, \bar{x}) > 0$.] This is a local type of stability analysis. For nonhyperbolic critical points, stability depends on nonlinear terms in the Taylor expansion of the vector field. Numerical analysis using AUTO is covered in detail by Doedel et al.,[20,21] and an introduction to continuation methods is given by Seydel.[22]

Equation (33) is recast as a system of coupled, first-order ODEs,

$$\dot{y}_i = y_{i+n\,\mathrm{mode}}$$

$$\dot{y}_{i+n\,\mathrm{mode}} = -\left(\frac{\mu\lambda}{M_\infty}\right)^{\frac{1}{2}} y_{i+n\,\mathrm{mode}} + CP\,y_i(i\pi)^2 - y_i(i\pi)^4 - \lambda\left[F_i^1(y_i)\right] - 3\left[\sum_{k=1}^{n\,\mathrm{mode}} y_k^2(k\pi)^2\right] y_i(i\pi)^2 + \frac{h}{a}\frac{\tilde{R}_u}{1-\nu}\left(\frac{\mu}{\lambda M_\infty}\right)^{\frac{1}{2}}\left[F_i^2(y_{i+n\,\mathrm{mode}})\right] y_i(i\pi)^2 \tag{35}$$

where $i = 1, 2, \ldots, n$ mode and n mode is the number of Galerkin modes retained in the formulation. The nondimensional in-plane load represented by CP, i.e., a free parameter here, is given as

$$CP = \left[R_f\left(\frac{\gamma-1}{2}\right)M_\infty^2\frac{T_\infty}{T_{cr}} + \left(\frac{T_\infty - T_{\mathrm{ref}}}{T_{cr}}\right)\right]\Theta = 3116.7 \times R_f - 321.3 \tag{36}$$

Also, the $F_i^1(y_i)$ are nonlinear functions associated with the geometric nonlinearity, whereas the $F_i^2(y_{i+n\,\mathrm{mode}})$ are linear functions of the generalized velocities. Both F_i^1 and F_i^2 are straightforward to generate.

Attractors and Bifurcations

Figure 3a shows a partial system bifurcation diagram for the equilibrium solutions. The ordinate $U(1)$ is the displacement of the first generalized coordinate, and the diagram is traced out as a function of the steady in-plane load. $U(1)$ is used to represent the panel displacement, although to be correct, $w(x, t)$ is found by summing all of the generalized coordinates multiplied by their corresponding mode shapes as indicated in Eq. (32). In this case, the higher modes are found to have smaller amplitudes than for the first two modes (at least with regard to the stable equilibria). Notable events, highlighted with numbers in Fig. 3a, signify either bifurcations or branch endpoints. The diagram is incomplete in the sense that additional solution branches, indicated by the numbered labels, are not shown. This was done to simplify Fig. 3a. It can be shown that all equilibrium branches not shown are unstable and are, therefore, of secondary importance to this study. The flat stable solution encounters a supercritical pitchfork bifurcation for $CP \approx 11.7$. This event is

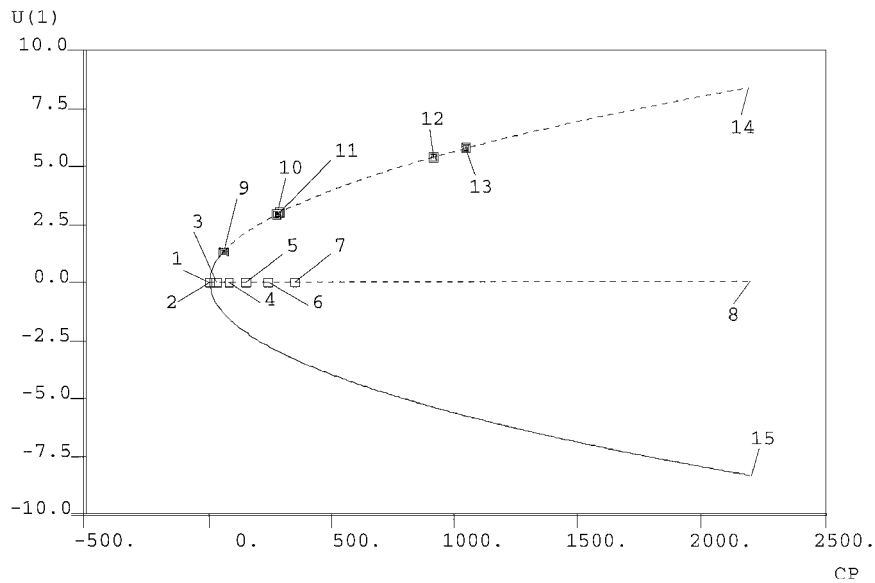

a) Six-mode model, $\lambda = 52.6$, $R_u = 0.5$

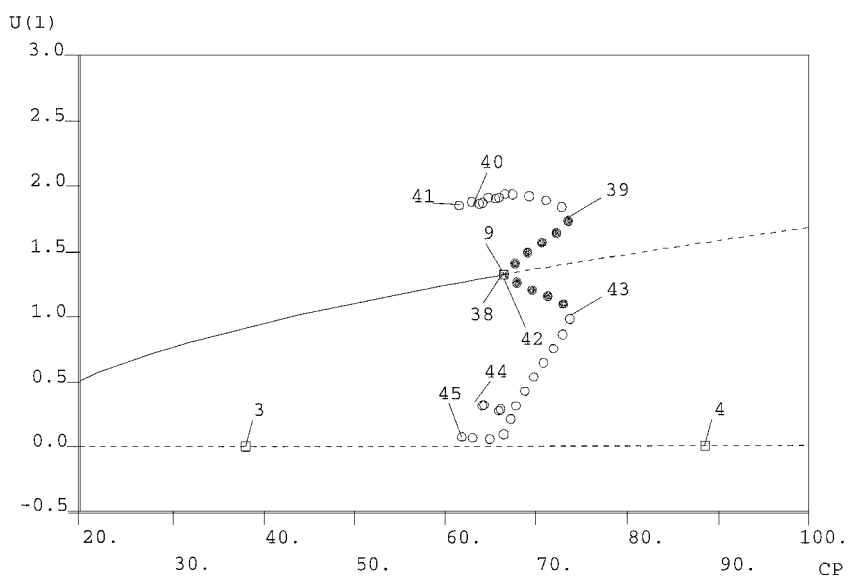

b) Periodic solution

Fig. 3 Bifurcation diagram for $R_u = 0.5$, $\lambda = 52.6$ indicating a) equilibrium solutions and b) Hopf bifurcation showing periodic solution. [Dots bound the minimum and maximum extent of $U(1)$ for the periodic motion.]

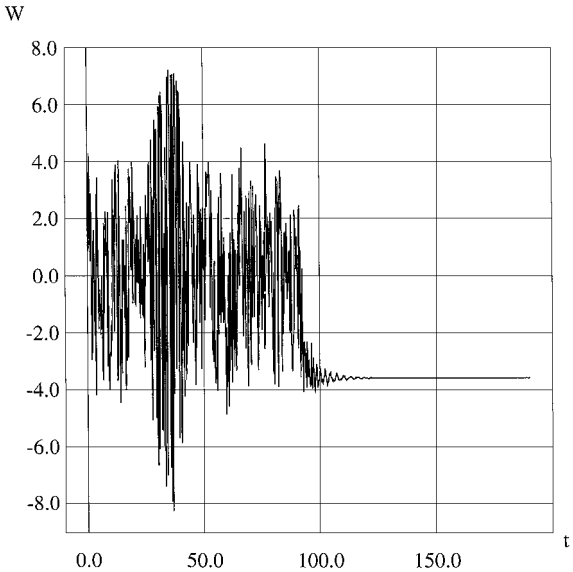

Fig. 4 Long-time history for stable equilibrium solution: $R_f = 0.293$, $R_u = 0.5$, dt = 5.e− 5.

noted as label 1 in Fig. 3a. Note, because only positive values of CP (corresponding to compressive stress) were considered, a local magnification, not shown, would be required to resolve this bifurcation. Stable equilibria are indicated with a solid line, whereas unstable equilibria are indicated with a dashed line. Open square symbols denote bifurcations to equilibria, whereas solid square symbols denote bifurcations to periodic motions.

In Fig. 3, $R_u = 0.5$. Thus, a portion of the unsteady thermal heating effect is included in the thermal stress model. For very small values of the control parameter, it is evident that both the up-buckled and down-buckled equilibrium solutions are stable. Of course, both solutions cannot exist simultaneously, and the initial condition will determine which solution is realized. The down-buckled solution branch is seen to continue uninterrupted as the control parameter is increased. Direct numerical integration verifies this behavior (Fig. 4). Note that the value of the recovery factor is indicated as $R_f = 0.293$. This corresponds to $CP \approx 600$. For the up-buckled branch, a supercritical Hopf bifurcation is encountered. The branch of stable periodic solutions emanating from the Hopf bifurcation (Fig. 3b, label 9) represents a limit cycle and is shown with solid dots. Stability can be determined by the moduli of the Floquet multipliers of the linearized Poincaré map. For the stable periodic solution, the extent of $U(1)$ is bounded, as indicated by the solid dots. As seen, the stable periodic regime is short lived and is terminated at a saddle node of periodic orbits.

To verify the AUTO results, the equations are numerically integrated with a fourth-order Runge–Kutta method. For values of the parameter for stable periodic motion indicated in Fig. 3b, the equivalent recovery factors are $R_f \in [0.1239, 0.1275]$. This rather small range for R_f should serve to emphasize that, to explore the parameter space in any detail with numerical integration only, an enormous computational program would be required. By using larger step increments in parameter space, many details of the attractors and bifurcations would be lost. For $R_f \simeq 0.1239$, a supercritical Hopf bifurcation is encountered. The trademark of this bifurcation is a limit cycle of zero amplitude as the bifurcation point is encountered. As the control parameter is increased, the amplitude of the limit cycle grows like the square root of the distance of the control parameter from the bifurcation point. To first order with respect to the control parameter, the period of the motion is constant. In Fig. 5a, the equilibrium solution is about to encounter a Hopf bifurcation. A small limit cycle is created as the bifurcation point is crossed. In Figs. 5b and 5c, the phase trajectory and power spectral density are shown. The limit cycle is structurally stable, and the amplitude grows as the control parameter is increased (Fig. 5d). The corresponding spectrum, not shown, is indeed constant with respect to distance from the bifurcation point. Eventually (Fig. 5e), the limit cycle becomes unstable and is replaced by an equilibrium solution. That is, for sufficient temperature rise in the panel additional heating stops the flutter motion, and the panel remains in the buckled-stable position.

The nondimensional frequency $\tilde{f}$ is approximately 6.25 and $\tilde{T} = 1/\tilde{f} = 0.16$. This is precisely the value of the period given by AUTO. Hence, results of the numerical integrations and AUTO are in full agreement. It is also of interest to compute the actual period T so that this characteristic time of oscillation may be compared to the characteristic thermal time. The period (in seconds) is related to the nondimensional period by

$$\tilde{T} = T/\tau, \qquad \tau = \sqrt{a^4 \rho_p h / D} = 0.16 \tag{37}$$

Hence $T = 0.0256$ s and $f = 1/T \approx 39$ Hz. Defining η as the ratio of the characteristic thermal time to the period of oscillation,

$$\eta = \frac{h^2/\alpha_D}{T} \approx 158$$

Therefore, for the small values of the in-plane load for which the limit cycle is stable, the period of vibration is $\mathcal{O}(10^2)$ smaller than the characteristic thermal time.

Perfect Thermal Communication

For $R_u = 1.0$, this condition implies that the fluid sublayer and panel are in perfect thermal communication. That is, the panel midplane unsteady temperature component follows the temperature change in the fluid sublayer with zero phase lag. Also, the unsteady temperature contribution is increased. Thus, for a buckled-stable panel and prior to any fluttering motion, the panel temperature is increased due to the profile shape term in Eq. (14). This makes the panel more susceptible to flutter. Hence, the stable Hopf bifurcation should be encountered earlier with respect to the control parameter. This is shown in Fig. 6a (label 9). Figure 6b shows the evolution of the stable periodic solution. As was the case for $R_u = 0.5$, all other periodic solution branches represent unstable periodic motions, for example, at label 10. The corresponding steady recovery factor is $R_f \in [0.1090, 0.1108]$. The frequency of the motion very near to the bifurcation point is approximately 11.1 Hz. Just before the periodic solution becomes unstable, it is 7.4 Hz. Hence, $\eta \approx 45$. Therefore, the characteristic thermal conduction time is still an order of magnitude larger than the period of oscillation even when the fluid sublayer and panel are assumed to be in perfect thermal communication. These results have been verified by direct numerical integration but are not shown here for brevity.

Time Constants for the Dynamical System

The results so far show that the characteristic thermal conduction time is at least an order of magnitude larger than the period of oscillation. This result is exacerbated as the frequency of oscillation increases. This suggests that unsteady thermal effects may be negligible. On the basis of this physical argument, it would appear reasonable to exclude the unsteady thermal contribution in the thermal stress calculation. Therefore, the continuation method is applied to the aerothermoelastic model but with the unsteady thermal model removed ($R_u = 0$). The modified model is similar in form to that given in Eq. (35). The bifurcation diagram is shown in Fig. 7. Blowups of this bifurcation diagram would reveal additional details. However, as was the case earlier, the additional solution branches were found to be unstable and, therefore, unrealizable; hence, they are not shown here. It is seen that the response is dominated by a stable fixed-point attractor. Additionally, both the up-buckled and down-buckled branches are stable throughout the entire parameter range. Furthermore, no bifurcations to periodic solution branches are encountered. Note, it can be shown that the bifurcation diagram for the six-mode classical panel flutter model is qualitatively similar to that shown in Fig. 7.

Finally, an eight-mode modified aerothermoelastic panel flutter model is analyzed using the continuation method. The bifurcation diagram, not shown here, is similar to that shown in Fig. 7 with the exception that two additional bifurcations to equilibria are seen. However, the branches are unstable and, therefore, unrealizable. All other details (including critical points and amplitudes) are similar with regard to the six-mode model. This indicates that six modes will accurately represent panel flutter behavior.

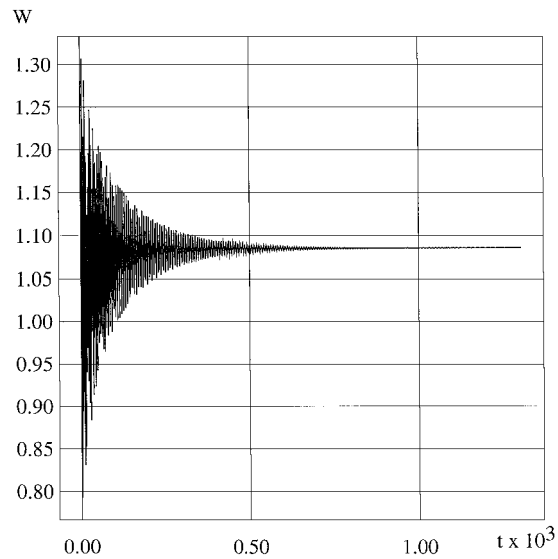

a) $R_f = 0.1239, R_u = 0.5$

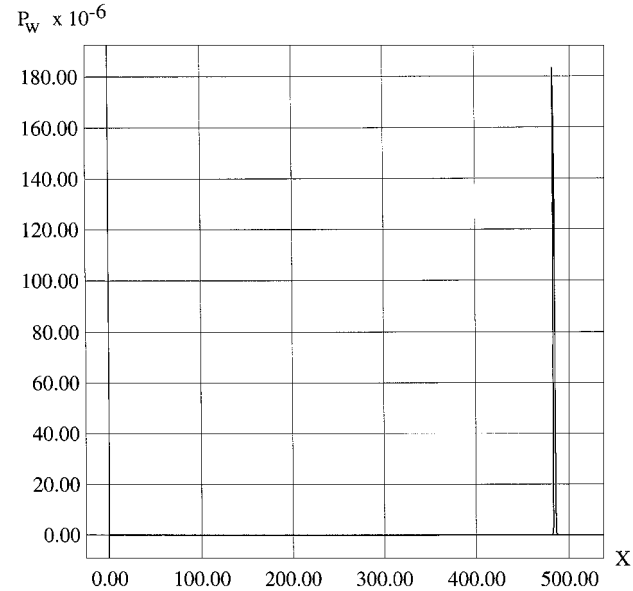

c) $R_f = 0.1246, R_u = 0.5$

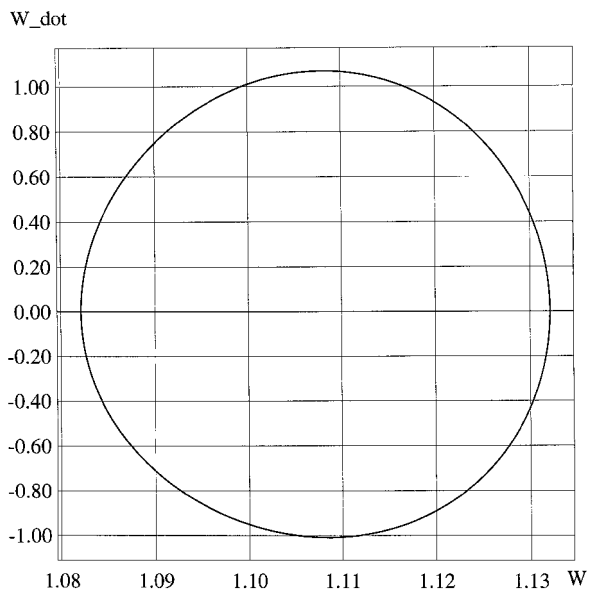

b) $R_f = 0.1246, R_u = 0.5$

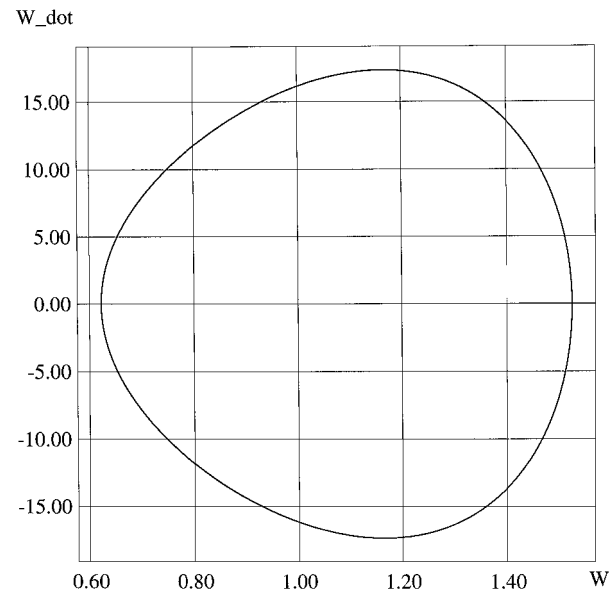

d) $R_f = 0.1268, R_u = 0.5$

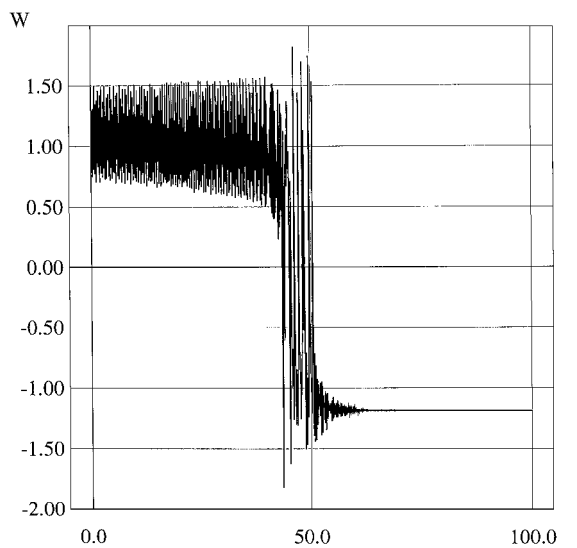

e) $R_f = 0.1272, R_u = 0.5$

Fig. 5 Evolution of supercritical Hopf bifurcation for six-mode aerothermoelastic panel flutter model: $R_u = 0.5$ and $\lambda = 52.6$.

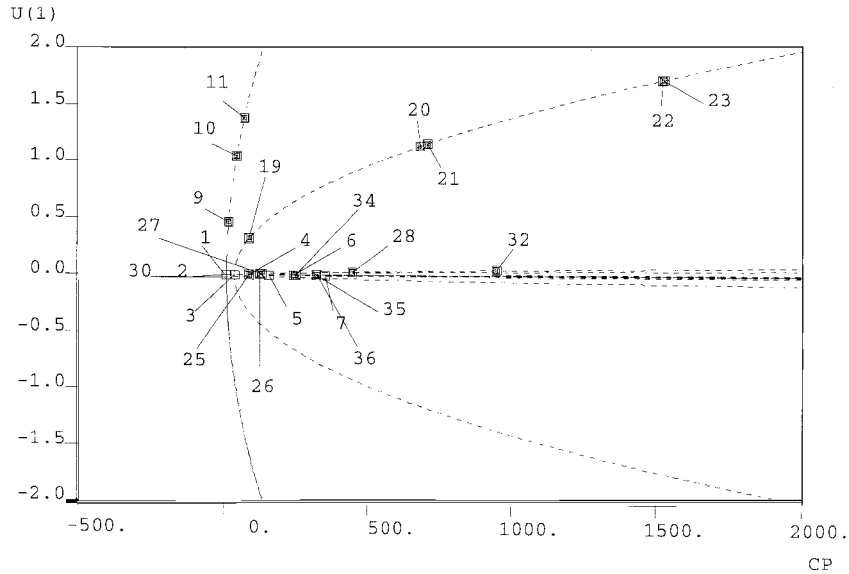

a) Six-mode model, $\lambda = 52.6$, $R_u = 1.0$

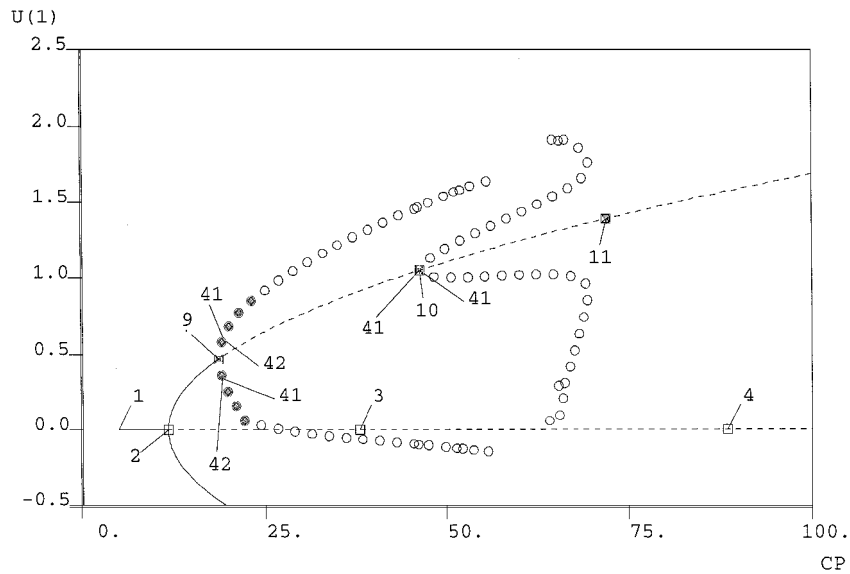

b) Periodic solution

Fig. 6 Bifurcation diagram for $R_u = 1.0$, $\lambda = 52.6$ indicating a) equilibrium and b) periodic solutions.

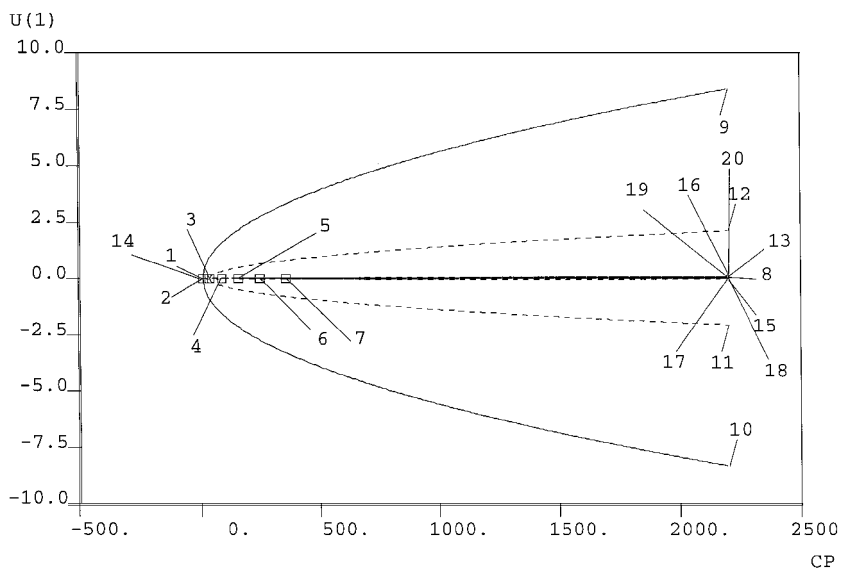

Fig. 7 Bifurcation diagram for $R_u = 0$, $\lambda = 52.6$ indicating equilibrium solutions for six-mode modified aerothermoelastic panel flutter model: ——, stable, and - - - -, unstable.

Conclusion

A nonlinear panel flutter formulation has been developed that includes two distinct heat transfer mechanisms. One is a steady viscous effect due to aerodynamic heating, and the other can be thought of as a time-dependent inviscid effect due to local flow over the panel. When the panel is flat stable, the latter term does not contribute to heating of the panel. In this formulation, two main parameters for panel flutter (compressive stress and a dynamic pressure parameter) are not wholly independent but are coupled to the external conditions. The static and postflutter behavior have been analyzed by direct numerical integration and by application of a numerical continuation procedure. The latter procedure is especially efficient with respect to numerical integration when the parameter space under consideration is large, as it is here. Fundamentally, this is because the solution space is mapped out from a known solution rather than an initial condition. In this way, the transient portion of any calculation is avoided. Indeed, the differential equation is not integrated at all. A new periodic attractor is uncovered and is shown to be due to inclusion of the inviscid heat transfer mechanism formulated here. However, it is shown that the characteristic time of oscillation is at least an order of magnitude smaller than the characteristic thermal conduction time. Hence, it appears reasonable to neglect the inviscid model altogether. In this way, it is shown that aerodynamic heating is the dominant heat transfer mechanism of the two considered.

Appendix A: Nondimensional Variables

The nondimensional variables are as follows:

$$
\begin{aligned}
\tilde{w} &= w/h \\
\tilde{x} &= x/a \\
R_x^E &= a^2 N^E/D \\
\tilde{t} &= t/\tau,\ \tau = \sqrt{(a^4 \rho_p h/D)} \\
D_t w &= (w_{,x} + w_{,t}/U_\infty) \\
\tilde{D}_t w &= (a/h) D_t w = [\tilde{w}_{,\tilde{x}} + (\mu/\lambda M_\infty)^{1/2} \tilde{w}_{,\tilde{t}}] \\
\mu &= \rho_\infty a/\rho_p h \\
\tilde{T} &= T/T_c, \\
T_c &= D/(Eha^2\alpha_p) \\
\Delta\tilde{T}_f &= (\tilde{T}_\infty - \tilde{T}_{\text{ref}}) + \tilde{R}_f \\
\Delta\tilde{T}_u &= \tilde{R}_u \tilde{D}_t w \\
\tilde{R}_f &= R_f(\gamma - 1)/2M_\infty^2 \tilde{T}_\infty \\
\tilde{R}_u &= R_u(\gamma - 1) M_\infty \tilde{T}_\infty \\
\Delta\tilde{p} &= \Delta p/p_c,\ p_c = Dh/a^4 \\
\Theta &= 1 - (\alpha_s + R\alpha_p)/[\alpha_p(\beta_k + R)]
\end{aligned}
$$

Note that $\tilde{T}_\infty$ is taken at altitude and $\tilde{T}_{\text{ref}}$ is referenced to sea level.

Appendix B: Material Properties for Rene-41

Table B1 Properties

Parameter	Value
Density, kg/m^3	8250
Poisson ratio	0.31
Coefficient of thermal expansion, $^\circ$C^{-1}	14.3e−06
Young's modulus, GPa	217.9
Thermal diffusivity, m^2/s	3.97e−06
R	0.2
k_s, GPa	1.0

Acknowledgment

The authors wish to thank Luigi Morino for valuable discussions on this work.

References

[1] Dugundji, J., "Theoretical Considerations of Panel Flutter at High Supersonic Mach Numbers," *AIAA Journal*, Vol. 4, No. 7, 1966, pp. 1257–1266.

[2] Ashley, H., and Zartarian, G., "Piston Theory—A New Aerodynamic Tool for the Aeroelastician," *Journal of the Aeronautical Sciences*, Vol. 23, No. 12, 1956, pp. 1109–1118.

[3] Dowell, E. H., "Nonlinear Oscillations of a Fluttering Plate," *AIAA Journal*, Vol. 4, No. 7, 1966, pp. 1267–1275.

[4] Dowell, E. H., "Nonlinear Oscillations of a Fluttering Plate II," *AIAA Journal*, Vol. 5, No. 10, 1967, pp. 1856–1862.

[5] Bolotin, V. V., *Nonconservative Problems of the Theory of Elastic Stability*, Pergamon, Oxford, England, UK, 1963, pp. 231–247.

[6] Kuo, C. C., and Morino, L., "Perturbation and Harmonic Balance Methods for Nonlinear Panel Flutter," *AIAA Journal*, Vol. 10, No. 11, 1972, pp. 1479–1484.

[7] Virgin, L. N., and Dowell, E. H., "Nonlinear Elasticity and Chaos," *Computational Nonlinear Mechanics in Aerospace Engineering*, edited by S. N. Atluri, Vol. 146, Progress in Aeronautics and Astronautics, AIAA, Washington, DC, 1992, p. 531.

[8] Sipcic, S. R., and Morino, L., "Dynamic Behavior of the Fluttering Panel on a Maneuvering Airplane," *AIAA Journal*, Vol. 29, No. 8, 1991, pp. 1304–1312.

[9] Sipcic, S. R., "Chaotic Response of Fluttering Panel the Influence of Maneuvering," *Nonlinear Dynamics 1*, 1990, pp. 243–264.

[10] Hedgepeth, J. M., "Flutter of Rectangular Simply Supported Panels at High Supersonic Speeds," *Journal of the Aeronautical Sciences*, Vol. 24, No. 8, 1957, pp. 563–573.

[11] Bein, T., Friedmann, P., Zhong, X., and Nydick, I., "Hypersonic Flutter of a Curved Shallow Panel with Aerodynamic Heating," AIAA Paper 93-1318, April 1993.

[12] Fung, Y. C., "The Static Stability of a Two Dimensional Curved Panel in a Supersonic Flow with an Application to Panel Flutter," *Journal of the Aeronautical Sciences*, Vol. 21, No. 8, 1954, pp. 556–565.

[13] Schaeffer, H. G., and Heard, W. L., Jr., "Flutter of a Flat Panel Subjected to a Nonlinear Temperature Distribution," *AIAA Journal*, Vol. 3, No. 10, 1965, pp. 1918–1923.

[14] Kordes, E. E., Tuovila, W. J., and Guy, L. D., "Flutter Research on Skin Panels," NASA TN-D-451, Sept. 1960.

[15] Guy, L. D., and Bohon, H. L., "Flutter of Aerodynamically Heated Aluminum-Alloy and Stainless-Steel Panels with Length-Width Ratio 10 at Mach Number 3.0," NASA TN-D-1353, July 1962.

[16] Schlichting, H., *Boundary-Layer Theory*, McGraw–Hill, New York, 1979, pp. 314–318.

[17] Hildebrand, F. B., *Advanced Calculus for Applications*, Prentice–Hall, Englewood Cliffs, NJ, 1976, pp. 463–466.

[18] Holman, J. P., *Heat Transfer*, 8th ed., McGraw–Hill, New York, 1997, pp. 140–144.

[19] Gee, D. J., "A Thermal Model for Nonlinear Panel Flutter," Ph.D. Dissertation, Dept. of Aerospace and Mechanical Engineering, Boston Univ., Boston, MA, July 1997.

[20] Doedel, E. J., Wang, X. J., and Fairgrieve, T., "AUTO94: Software for Continuation and Bifurcation Problems in Ordinary Differential Equations," Applied Mathematics Rept. CRPC-95-2, California Inst. of Technology, Pasadena, CA, March 1995.

[21] Doedel, E., Keller, H. B., and Kernevez, J. P., "Numerical Analysis and Control of Bifurcation Problems: (II) Bifurcation in Infinite Dimensions," *International Journal of Bifurcation and Chaos*, Vol. 1, No. 4, 1991, pp. 745–771.

[22] Seydel, R., "Tutorial on Continuation," *International Journal of Bifurcation and Chaos*, Vol. 1, No. 1, 1991, pp. 3–11.

G. A. Kardomateas
Associate Editor